NEUROSCIENCE

A gut-brain axis mediates sodium appetite via gastrointestinal peptide regulation on a medulla-hypothalamic circuit

Yuchu Liu[1,2]†, Ji-an Wei[1,2]†, Zhihua Luo[1]†, Jing Cui[1], Yifan Luo[2], Sarah Oi Kwan Mak[2], Siqi Wang[1], Fengwei Zhang[2], Yan Yang[1], Kwok-Fai So[1,3,4,5], Lingling Shi[1]*, Li Zhang[1,3,4]*, Billy Kwok Chong Chow[2]*

Salt homeostasis is orchestrated by both neural circuits and peripheral endocrine factors. The colon is one of the primary sites for electrolyte absorption, while its potential role in modulating sodium intake remains unclear. Here, we revealed that a gastrointestinal hormone, secretin, is released from colon endocrine cells under body sodium deficiency and is indispensable for inducing salt appetite. As the neural substrate, circulating secretin activates specific receptors in the nucleus of the solitary tracts, which further activates the downstream paraventricular nucleus of the hypothalamus, resulting in enhanced sodium intake. These results demonstrated a previously unrecognized gut-brain pathway for the timely regulation of sodium homeostasis.

INTRODUCTION

Water and salt homeostasis is crucial for the survival of terrestrial animals. By continuously monitoring the sodium content of body fluids, mammals can maintain salt homeostasis via both neural circuits and hormonal factors. Within the brain, the subfornical organ (SFO) and the nucleus of the solitary tract (NTS) sense salt contents in cerebrospinal fluid (CSF) and initiate sodium intake behaviors (*1*–*4*). As an alternative neural mechanism, serotonin 2C receptor (Htr2c) neurons in the lateral parabrachial nucleus (LPBN) can suppress sodium appetite by projecting to the central amygdala (CeA) (*5*).

In terms of endocrine factors, angiotensin II (ANG II) binds to the zona glomerulosa (ZG) under sodium deficiency (*6*), inducing the release of aldosterone (*7*, *8*) to mediate sodium reabsorption in the distal nephron of the kidney (*9*). In the brain, ANG II type 1 receptor (AT1aR) neurons in the SFO project to the dorsal bed nucleus of the stria terminalis (dBNST) to induce salt intake (*10*). The exact role of circulating ANG II in centrally mediating salt appetite is still controversial (*11*, *12*), although the blood-brain barrier (BBB) permeability of ANG II was relatively high (*13*). In the NTS, sodium appetite is also regulated by aldosterone-sensitive 11-β-hydroxysteroid dehydrogenase type 2 (HSD2) neurons (*1*), which project to pre-locus coeruleus (p-LC) prodynorphin (PDYN) neurons (*14*), the medial subdivision of the central lateral parabrachial nucleus (mPBcl) and the bed nucleus of the stria terminalis (BNST) (*3*, *15*). However, the permeability of aldosterone across the BBB is relatively low (*16*–*18*), raising the possibility of other neuropeptides forming a peripheral-central axis for salt intake.

Inside the body, sodium absorption in the food chyme primarily occurs within the gastrointestinal (GI) tract, which abundantly expresses sodium channels (*19*). These observations raise one interesting question: Can the GI tract respond to body sodium levels and then transduce this signal to the brain to mediate salt appetite? However, no neural or hormonal pathway has been reported to support this model. The GI peptide secretin (SCT) was previously found to participate in renal water reabsorption by mediating vasopressin expression (*20*) and hypothalamic regulation of water intake (*21*). SCT owned prominent expression levels in colon tissues (*22*, *23*) and satisfactory BBB permeability (*24*). We thus proposed that SCT might work as a neuropeptide to modulate salt intake in a response to body sodium levels.

To test this hypothesis, we identified elevated SCT levels in the colon mesenchyme under low-sodium stress, and the release of SCT is necessary for inducing salt intake. To dissect the neural substrate, the SCT receptor (SCTR) was found in a specific neuronal subpopulation in the NTS, which was activated upon elevated peripheral or central SCT. Optogenetic and chemogenetic manipulation of these NTS-SCTR$^+$ cells validated their roles in facilitating salt intake under sodium depletion, via monosynaptic projection to the paraventricular nucleus of the hypothalamus (PVH). In summary, we revealed a previously recognized gut-brain axis by which colon SCT responds to salt deficiency and stimulates salt intake.

[1]Key Laboratory of CNS Regeneration (Ministry of Education), Guangdong-Hong Kong-Macau Institute of CNS Regeneration, Jinan University, Guangzhou, China. [2]School of Biological Sciences, University of Hong Kong, Hong Kong SAR, China. [3]Center for Brain Science and Brain-Inspired Intelligence, Guangdong-Hong Kong-Macao Greater Bay Area, Guangzhou, China. [4]Neuroscience and Neurorehabilitation Institute, University of Health and Rehabilitation Sciences, Qingdao, China. [5]State Key Laboratory of Brain and Cognitive Science, Li Ka Shing Faculty of Medicine, University of Hong Kong, Hong Kong SAR, China.
†These authors contributed equally to this work.
*Corresponding author. Email: zhangli@jnu.edu.cn (L.Z.); bkcc@hku.hk (B.K.C.C.); tlingshi@jnu.edu.cn (L.S.)

RESULTS

Circulating SCT mediates salt appetite under acute sodium depletion

To generate a sodium-deficient (Na-D) model, mice were injected with furosemide (50 mg/kg) to induce sodium loss (*25*), followed by a low-sodium diet for 24 hours (Fig. 1A). These Na-D mice showed a strong appetite for 3% saline during the first 30 min in the two-bottle test, while sodium-satisfied (control, or Na-S) mice did not

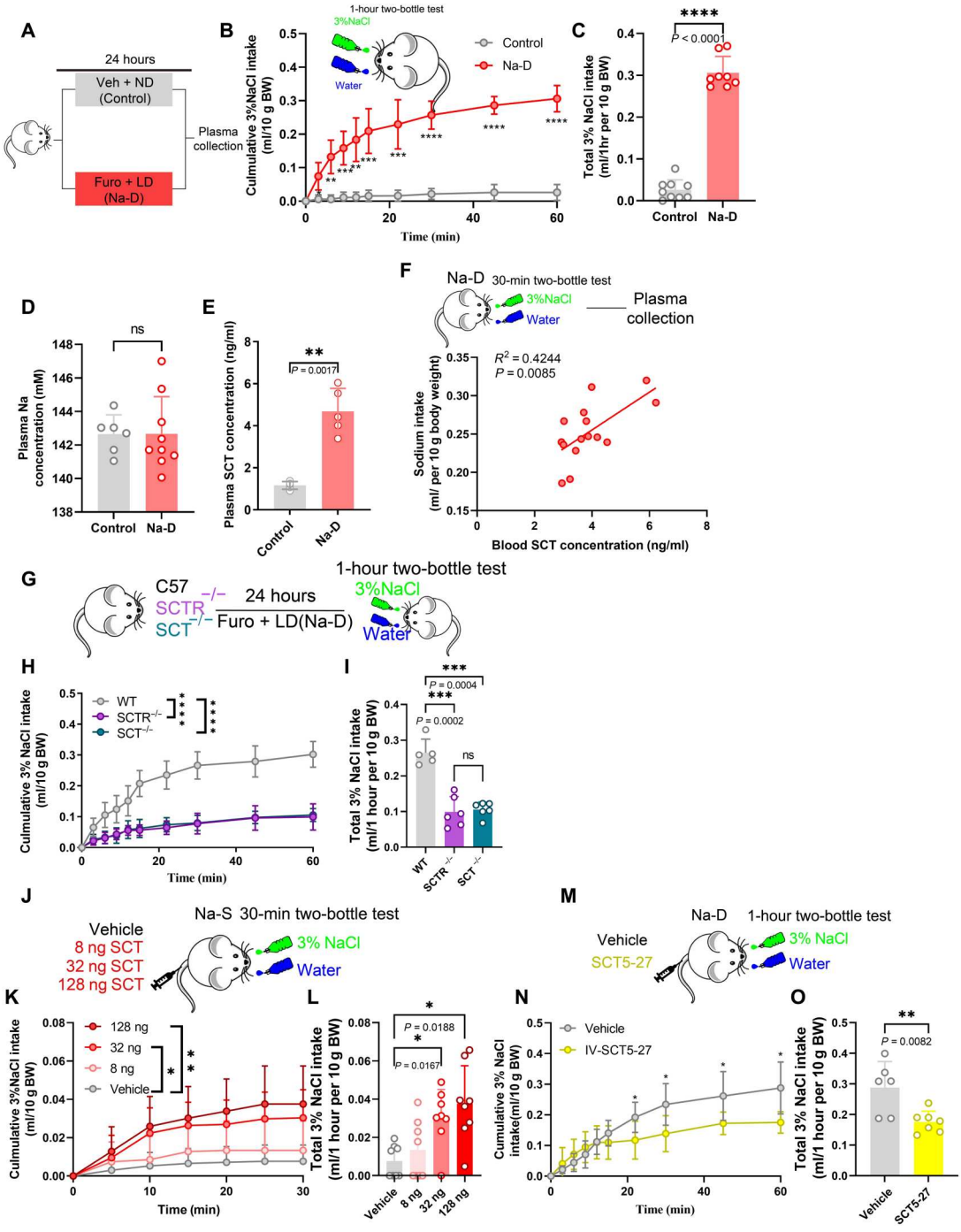

Fig. 1. Sodium depletion raised serum SCT to stimulate salt appetite. (**A**) Schematic diagram of sodium deficiency (Na-D) treatment. (**B**) Comparison of 1-hour cumulative saline intake under Na-D and Na-S. Two-way ANOVA, group factor $F_{1,15} = 181.4$, $P < 0.0001$. BW, body weight. (**C**) Quantification of saline intake during 1-hour two-bottle test. Unpaired Student's *t* test, $P < 0.0001$; $n = 9$ and 8 mice for the control group and Na-D group, respectively, in (B) and (C). (**D**) Plasma sodium concentration did not show any change after Na-D treatment. Welch's *t* test, $t = 0.02097$; $n = 6$ and 8 mice for the control group and Na-D group, respectively. (**E**) Serum SCT concentration was increased after Na-D treatment. Welch's *t* test, $t = 7.102$; $n = 5$ mice in each group. (**F**) Correlation between serum SCT concentration and sodium intake under Na-D. (**G**) Schematic diagram of two-bottle behavior test in transgenic mice. (**H**) Comparison of 1-hour cumulative saline intake under Na-D in C57, $SCTR^{-/-}$, or $SCT^{-/-}$ mice. (**I**) Quantification of saline intake during 1-hour two-bottle test. $n = 5$, 6, and 6 mice for control, $SCT^{-/-}$, and $SCTR^{-/-}$ group, respectively. (**J**) Schematic diagram of SCT injection assay. (**K**) Comparison of 1-hour cumulative saline intake after 8, 32, and 128 ng of SCT or vehicle injection under Na-S condition. Two-way ANOVA, group factor $F_{3,28} = 6.511$, $P < 0.0001$. (**L**) Quantification of saline intake during 1-hour two-bottle test. One-way ANOVA, $F_{3,28} = 6.874$, $P < 0.0001$. $n = 8$ mice in each group in (K) and (L). (**M**) Schematic diagram of SCT5-27 administration using Na-D mice. (**N**) Comparison of 1-hour cumulative intakes of 3% saline in 1.5-μg SCT5-27 injection mice under Na-D. (**O**) Quantification of saline intake during the 1-hour two-bottle test. Student *t* test, $t = 8.217$. $n = 6$ and 8 mice in vehicle and STC5-27 group, respectively, in (N) and (O). *$P < 0.05$, **$P < 0.01$, ***$P < 0.001$, and ****$P < 0.0001$, with significant difference. All data were presented as means ± SD.

show such preference (Fig. 1, B and C). Moreover, the plasma sodium level remained unchanged after furosemide treatment (Fig. 1D), in an agreement with a previous study (*26*). Sodium appetite can be driven by either neural or endocrine pathways. Peripheral organs, including the GI tract, affect brain activity via the vagal afferent nerve (*27*, *28*), which may also participate in the central regulation of sodium intake. We thus performed the vagotomy on Na-D–treated mice to disconnect GI organs from the brain (fig. S1, A and B). The absence of wheat germ agglutinin (WGA) labeling (*29*) in the dorsal motor nucleus (fig. S1, C to E) demonstrated the efficiency of the vagotomy, which, however, did not affect the volume or preference toward saline (fig. S1, F and G). Although recent works also suggested the involvement of spinal afferent pathway in gut-brain communications (*30*), we proposed that salt appetite is primarily mediated by a hormonal pathway under Na-D. This hypothesis was supported by the observation that sodium deficiency was associated with an elevated SCT concentration (Fig. 1, E and F).

To demonstrate the causal relationship between SCT and salt appetite, we used null knockout mice [$SCT^{-/-}$ and $SCTR^{-/-}$; see (*31*)], which showed decreased saline intake and the absence of sodium preference under Na-D conditions (Fig. 1, G to I). As an alternative approach to manipulate the SCT pathway, we peripherally infused gradient amounts of recombinant SCT peptide (8, 32, or 128 ng) to stimulate saline drinking in Na-S mice (Fig. 1J). The infusion of SCT peptides elevated the preference toward 3% saline (Fig. 1, K and L), which was not physiologically required. Moreover, the infusion of the SCTR antagonist SCT5-27 (1.5 μg) (*32*) decreased the total saline intake of Na-D mice (Fig. 1, M to O). These results suggested that circulating SCT facilitated salt intake under Na-D stress.

Colon tissues respond to sodium challenge by releasing SCT to elicit salt appetite

As one GI peptide, SCT is abundantly expressed in the duodenum (*33*), small intestine (*34*), and colon tissues (*35*). To investigate the origin of circulating SCT under Na-D, we generated an SCT-Cre;ROSA-tdTomato double-transgenic mouse line (*36*), in which SCT expression was found across different intestinal segments (Fig. 2A). However, only colon tissues showed significantly increased SCT mRNA and peptide levels under Na-D (Fig. 2, B and C). We thus hypothesized that colon SCT responds to low-sodium challenge to facilitate salt intake. Immunofluorescent labeling on SCT-Cre;ROSA-tdTomato mice identified prominent expression of SCT in enterochromaffin pancreozymin cells [tryptophan hydroxylase positive (TPH^+)] but not in fibroblasts ($vimentin^+$; Fig. 2, D and E), implying the neuroendocrine nature of SCT^+ cells, which were unaffected by mechanical contraction (*23*).

To better support the causal link between colon SCT and salt intake, we established a colon-specific *Sct* gene knockdown (KD) model by local injection of an adeno-associated virus (AAV) vector expressing small interference RNA (siRNA) targeting SCT transcript [AAV-CAG-siRNA (SCT)–green fluorescent protein (GFP)] into five different intestinal sites of mice under Na-D challenge (Fig. 2F). Immunofluorescent staining confirmed the region- and cell-type specificity of the virus in colon TPH^+ cells (Fig. 2G and fig. S2, A to D). Reduction of *Sct* gene expression was found in both the proximal and distal colon (fig. S2, E and F). *Sct* gene KD was further confirmed by quantitative polymerase chain reaction (qPCR) and enzyme-linked immunosorbent assays (ELISAs; Fig. 2, H and I). These mice presented normal water and food intake under naïve conditions and no signs of significant body weight gain/loss (fig. S3). The colon-specific deficiency of SCT (KD) did not affect the basal level of serum SCT but dampened the SCT surge under Na-D (Fig. 2J). The SCT concentration in CSF paralleled such changes in serum (Fig. 2K), suggesting potentially central functions. In the two-bottle test, colon-specific *Sct* gene KD decreased total saline intake (Fig. 2L) and largely abolished the saline preference (Fig. 2M) under Na-D challenge. Moreover, SCT KD in colons did not affect the local function of neuroendocrine cells or integrity of intestinal tissues, as suggested by unchanged *Tph1*, *Glp1*, or aquaporin (*Aqp*) genes (fig. S4). In another set of assays, the chemogenetic excitation of colon SCT^+ cells (fig. S5, A to E) elevated circulating SCT levels (fig. S5, F and G) and induced saline intake in Na-S mice (fig. S5, H and I). These results converged to suggest the role of colon-derived SCT in centrally mediating sodium intake.

$SCTR^+$ neurons in the NTS facilitate sodium intake

Given the elevated SCT level in CSF under Na-D, we investigated the neural mechanism of SCT in mediating salt intake. To centrally block the SCT pathway, the lateral ventricle was implanted with a cannula connected to an osmotic mini-pump prefilled with SCT antibody (Fig. 3, A to C). Under Na-D, the saline intake volume and preference were both depressed with SCT neutralization (Fig. 3, D and E), suggesting the role of brain SCTR during salt homeostasis. To better characterize the spatial distribution of SCTR, we generated an SCTR-Cre transgenic mouse line (fig. S6), which was further crossed with the ROSA-tdTomato (Ai9) reporter line to visualize the spatial patterns of SCTR expression (Fig. 3F). Apart from previous findings showing the presence of SCTR in the hippocampus, hypothalamus, and cerebellum (*21*), we quantified $SCTR^+$ cells in different nuclei related to water and salt homeostasis (Fig. 3, G to L). Among these regions, NTS had the highest expression level, while BNST, p-LC, the parabrachial nucleus (PBN), SFO, and PVH showed only minimal SCTR expression (Fig. 3M). Along the rostral-caudal axis of the NTS, the highest $SCTR^+$ cell density occurred in the subpostremal part of the NTS [spNTS; anterior-posterior (AP): −7.2 mm to AP: −7.48 mm; fig. S7]. To dissect the identity of NTS-$SCTR^+$ cells, RNAscope found that all $SCTR^+$ neurons were glutamatergic cells ($Vglut2^+$) and accounted for 37.6% of this population in the spNTS (Fig. 3, N and O).

Next, we analyzed the neuronal activity of NTS-$SCTR^+$ cells under Na-D. Using the immediate early gene cFos, we found the excitation of NTS-$SCTR^+$ neurons upon Na-D and under intravenous (IV) or intracerebroventricular (ICV) SCT infusion (Fig. 4, A and B). Furthermore, the activity of NTS-$SCTR^+$ cells was recorded using an ex vivo patch clamp (Fig. 4C), and SCT perfusion remarkably elevated the frequency of spikes at gradient dosage (Fig. 4, D and E), suggesting potentiated NTS excitability by SCT (fig. S8). These results illustrated the necessity of SCT-SCTR axis of the NTS in maintaining salt intake under Na-D.

Last, to track the in vivo activity of NTS-$SCTR^+$ neurons, an optic fiber was implanted into SCTR-Cre mice whose NTS was infected with genetically coded fluorescent calcium indicator GCaMP6s under a double-inverted orientation (DIO) flanking sequence (Fig. 5, A and B). After IV-SCT injection, elevated neural activity changes were observed within 10 min (Fig. 5, C and D). The activity of NTS-$SCTR^+$ neurons was further observed during fluid ingestion. No obvious calcium peak was found in Na-S mice

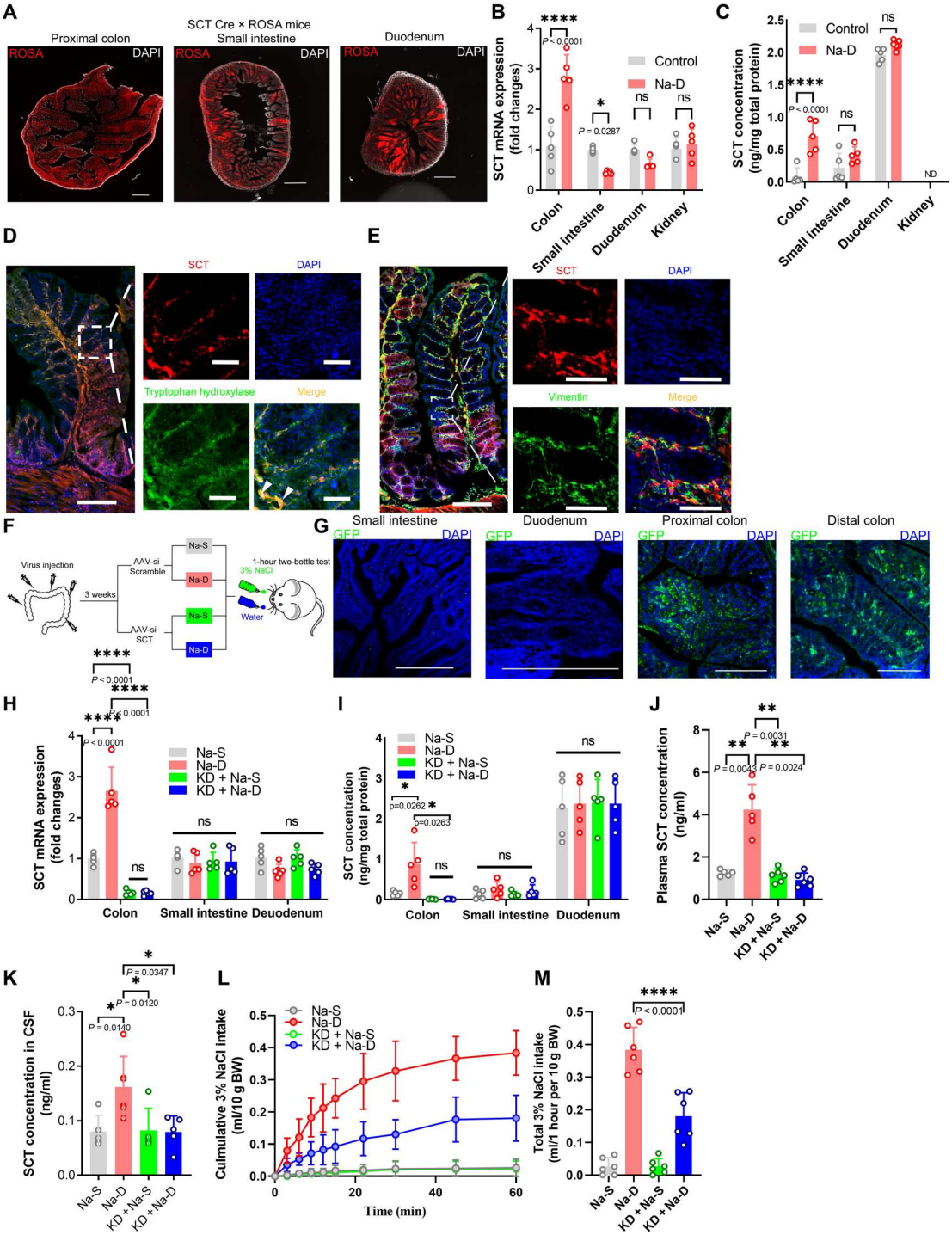

Fig. 2. Colon mesenchymal senses hyponatremia by biosynthesis of SCT. (**A**) Confocal images showing SCT expression in the colon, small intestine, and duodenum using SCT-Cre;ROSA-tdTomato double-transgenic mice. Scale bars, 500 μm. (**B**) Colon mRNA level of SCT was increased under Na-D conditions. Two-way ANOVA, group factor $F_{3,32} = 32.57$, $P < 0.0001$. (**C**) Na-D–induced colon secretion of SCT. $F_{2,25} = 388.6$, $n = 5$ mice for each group in (B) and (C). (**D** and **E**) Confocal images showing colon SCT$^+$ within enterochromaffin (TPH$^+$) cells, but not myofibroblasts/fibroblasts (vimentin$^+$). Scale bars, 200 μm (left) and 50 μm (right). DAPI, 4′,6-diamidino-2-phenylindole. (**F**) Schematic diagram of colon-specific KD of SCT. (**G**) Specific infection of siRNA-SCT-GFP virus in colon tissue. Scale bars, 200 μm. (**H**) mRNA level of SCT in the colon, small intestine, and duodenum under Na-S, Na-D, SCT KD in colon + normal diet (KD + Na-S), or KD + Na-D. $F_{2,50} = 1.343$, $P < 0.05$. (**I**) Na-D–induced SCT release was blocked by colon-specific SCT KD. $F_{3,48} = 2.221$, $P < 0.05$. (**J**) Na-D increased serum SCT, which was absent under colon-specific SCT KD. One-way ANOVA, $F_{3.5,295} = 31.62$, $P < 0.001$. $n = 5$ mice for each group in (H) to (J). (**K**) The Na-D-induced CSF SCT surge was not present in the colon-specific SCT KD group. $n = 5$ mice for each group. (**L**) Comparison of 1-hour cumulative saline intake. (**M**) Quantification of water and 3% saline intake during the 1-hour two-bottle test. SCT KD in colons led to decreased 3% saline intake. $n = 5$ mice for each group in (L) and (M). *$P < 0.05$, **$P < 0.01$, ***$P < 0.001$, and ****$P < 0.0001$, with significant difference. All data were presented as means ± SD.

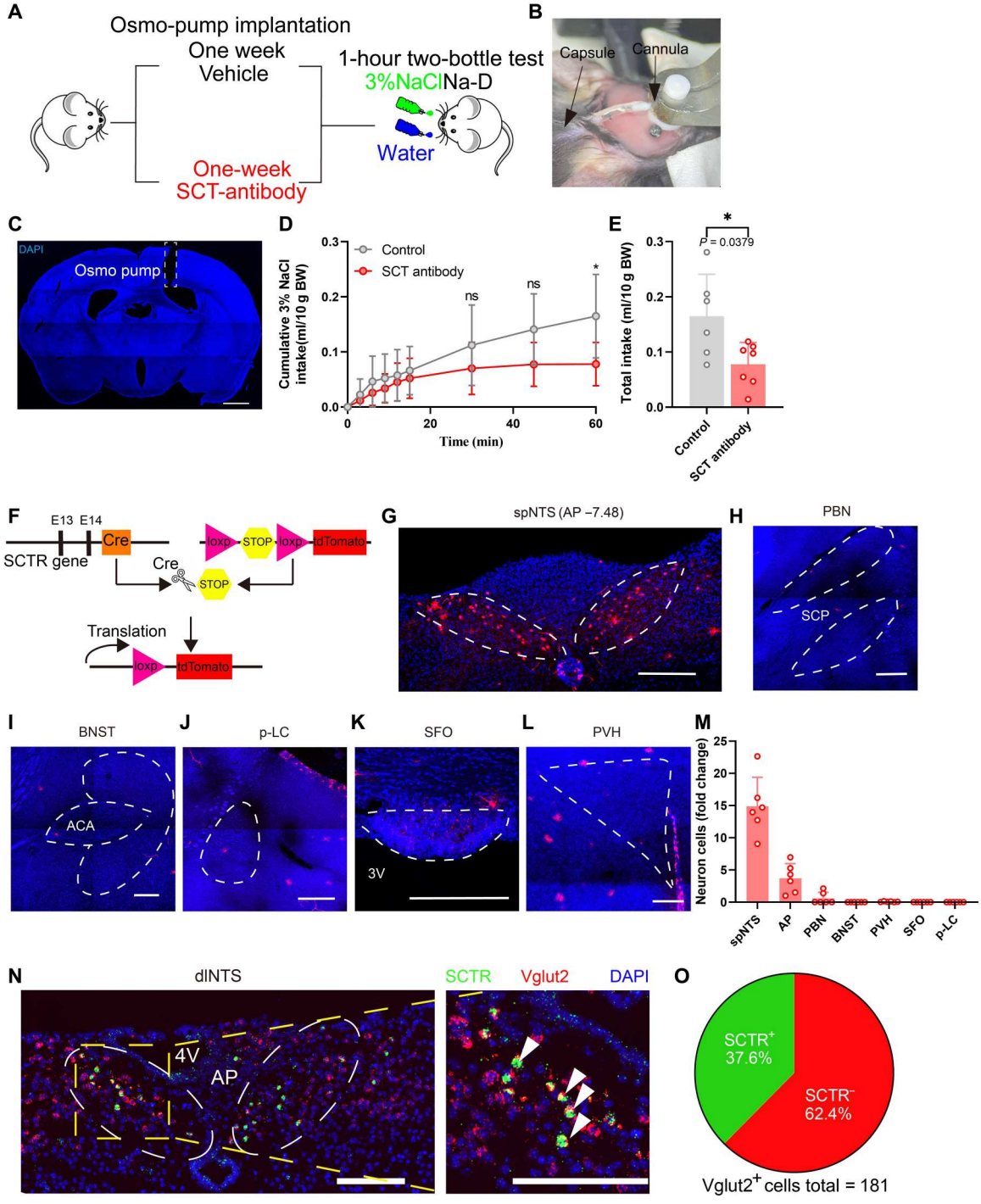

Fig. 3. SCT may mediate sodium intake via a central mechanism. (**A** to **C**) Schematic diagram of cannula implantation for SCT antibody infusion. The mini-osmotic pump was placed in a subcutaneous back pocket of the mouse. (**D**) Comparison of 1-hour cumulative 3% saline intake under SCT antibody infusion. $n = 7$ and 6 mice in the control and anti-SCT group, respectively. (**E**) Quantification of water and 3% saline intake during the 1-hour two-bottle test. SCT antibody decreased the saline intake. Unpaired Student's t test, $t = 2.660$, $n = 7$ and 6 mice in the control and anti-SCT group, respectively. (**F**) Schematic illustration of SCTR-Cre;ROSA-tdTomato double-transgenic mice. (**G** to **L**) Representative confocal images of SCTR$^+$ neurons in water and sodium homeostasis–related brain nuclei. Scale bars, 200 μm. (**M**) Quantification of SCTR$^+$ neurons across brain regions. $n = 6$ mice. (**N** and **O**) Representative images of multicolored RNAscope showed that most of NTS-SCTR$^+$ cells were Vglut2$^+$ neurons. Scale bars, 200 μm. $n = 6$ mice. *$P < 0.05$, **$P < 0.01$, ***$P < 0.001$, and ****$P < 0.0001$, with significant difference. All data were presented as means ± SD.

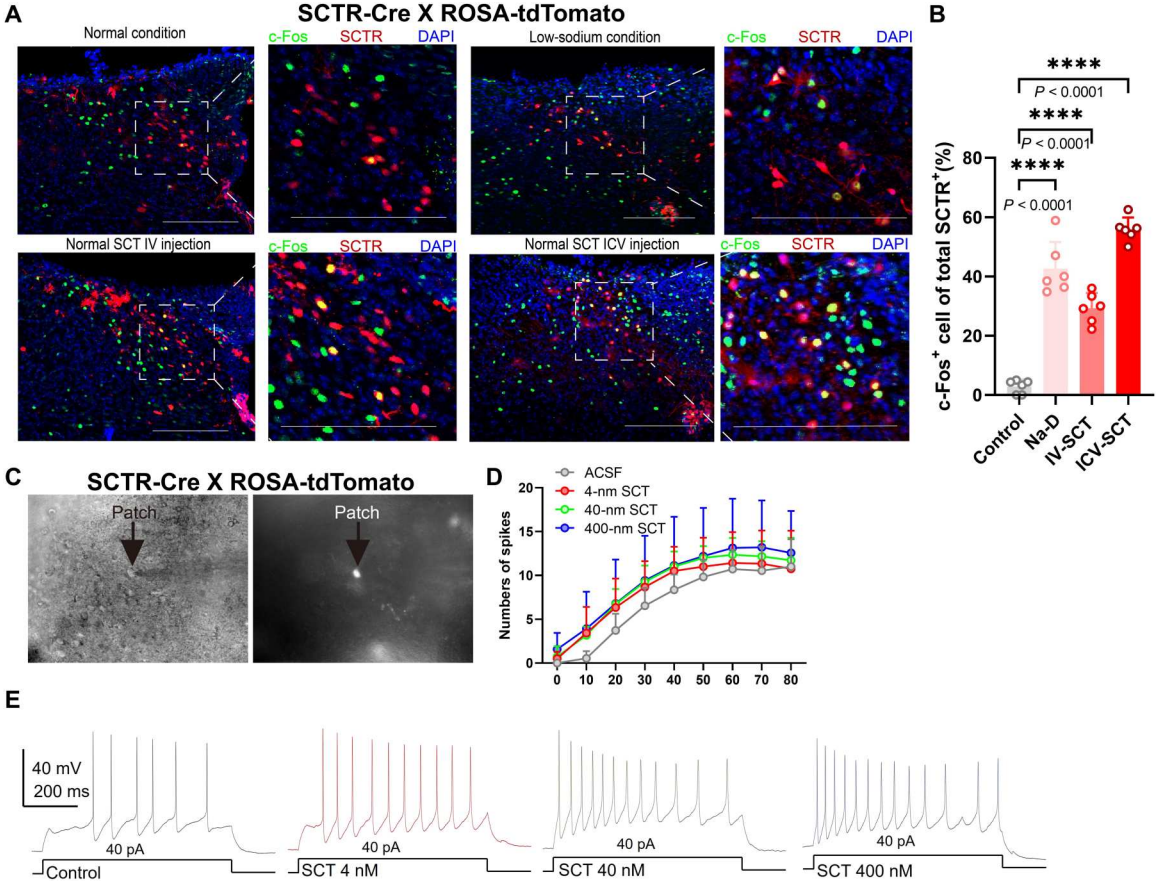

Fig. 4. NTS neurons are activated by SCT under sodium deficiency. (**A**) Representative confocal images showing c-Fos expression in SCTR$^+$ cells in dorsolateral NTS (dlNTS) using SCTR-Cre;ROSA-tdTomato mice. Scale bars, 200 μm. (**B**) Quantification of c-Fos$^+$ signals in SCTR$^+$ neurons under normal conditions, Na-D, 128-ng IV-SCT injection, or ICV-SCT injection. One-way ANOVA; $F_{3,20} = 1.187$. $n = 6$ mice in each group. (**C**) Sample images of electrophysiological recording in SCTR$^+$ neurons. (**D** and **E**) Quantification and representative spiking traces showing that SCT can activate SCTR$^+$ cells in the dlNTS. *$P < 0.05$, **$P < 0.01$, ***$P < 0.001$, and ****$P < 0.0001$, with significant difference. All data were presented as means ± SD.

regardless of whether saline, KCl, water, or oil was used (Fig. 5, E to G). However, Na-D mice showed remarkably decreased calcium activities of NTS-SCTR$^+$ neurons immediately after the first lick of saline but not for other fluids (Fig. 5, H to J). The depression of NTS-SCTR$^+$ neurons after satisfying sodium appetite further supported their roles in eliciting sodium appetite.

NTS-SCTR$^+$ neurons facilitated salt appetite via their hypothalamic projections

After recognizing the activation of NTS-SCTR$^+$ cells under sodium deficiency, we next tested the necessity of those cells in eliciting salt intake. First, the expression of SCTR was abolished by transfecting AAV-hSyn-Cre-tdTomato into the NTS of SCTR$^{fl/fl}$ mice (Fig. 6, A and B). The conditional knockout of SCTR suppressed saline intake (Fig. 6, C and D), suggesting the participation of SCT-SCTR axis in sodium appetite. Next, the role of NTS-SCTR$^+$ cells was evaluated by the cell ablation approach, in which AAV-DIO-Caspase3 was infected into the NTS of SCTR-Cre mice (Fig. 6, E to G). The removal of NTS-SCTR$^+$ cells resulted in decreased saline intake under Na-D (Fig. 6, H and I), suggesting their roles in facilitating sodium appetite. To better characterize the behavioral relevance, the excitatory chemogenetic receptor hM3Dq was expressed in the NTS of SCTR-Cre mice under the DIO flanked sequence (Fig. 6J). The injection of the receptor ligand clozapine *N*-oxide (CNO) elevated cFos activity in NTS neurons even under Na-S conditions (Fig. 6K) and induced saline intake (Fig. 6L) to produce salt preference (Fig. 6M), although sodium is not physiologically required at this moment. On the other hand, when NTS-SCTR$^+$ neurons were deactivated by the inhibitory receptor hM4Di and CNO infusion (Fig. 6, N and O), the total saline intake was repressed even under Na-D conditions (Fig. 6, P and Q). These results collectively illustrated the indispensable role of NTS-SCTR$^+$ neurons in facilitating salt intake under Na-D.

To depict the real-time effect of NTS-SCTR$^+$ cells during salt intake, we further used an optogenetic approach by infecting SCTR-Cre mice with AAV–DIO–channelrhodopsin-2 (ChR2) or halorhodopsin-3.0 (NpHR3.0; Fig. 6, R and U), followed by a two-bottle test with light stimulation via preimplanted optic fibers (fig. S9A). The light activation of NTS-SCTR$^+$ cells (fig. S9B) remarkably enhanced saline intake (Fig. 6S) even under Na-S conditions, without a remarkable effect on water drinking behaviors (Fig. 6T). In a second assay using Na-D mice that normally presented strong sodium appetite, light inhibition of NTS-SCTR$^+$ neurons (fig. S9B) strongly inhibited saline drinking behaviors (Fig. 6V), while leaving water intake unaffected (Fig. 6W). Furthermore,

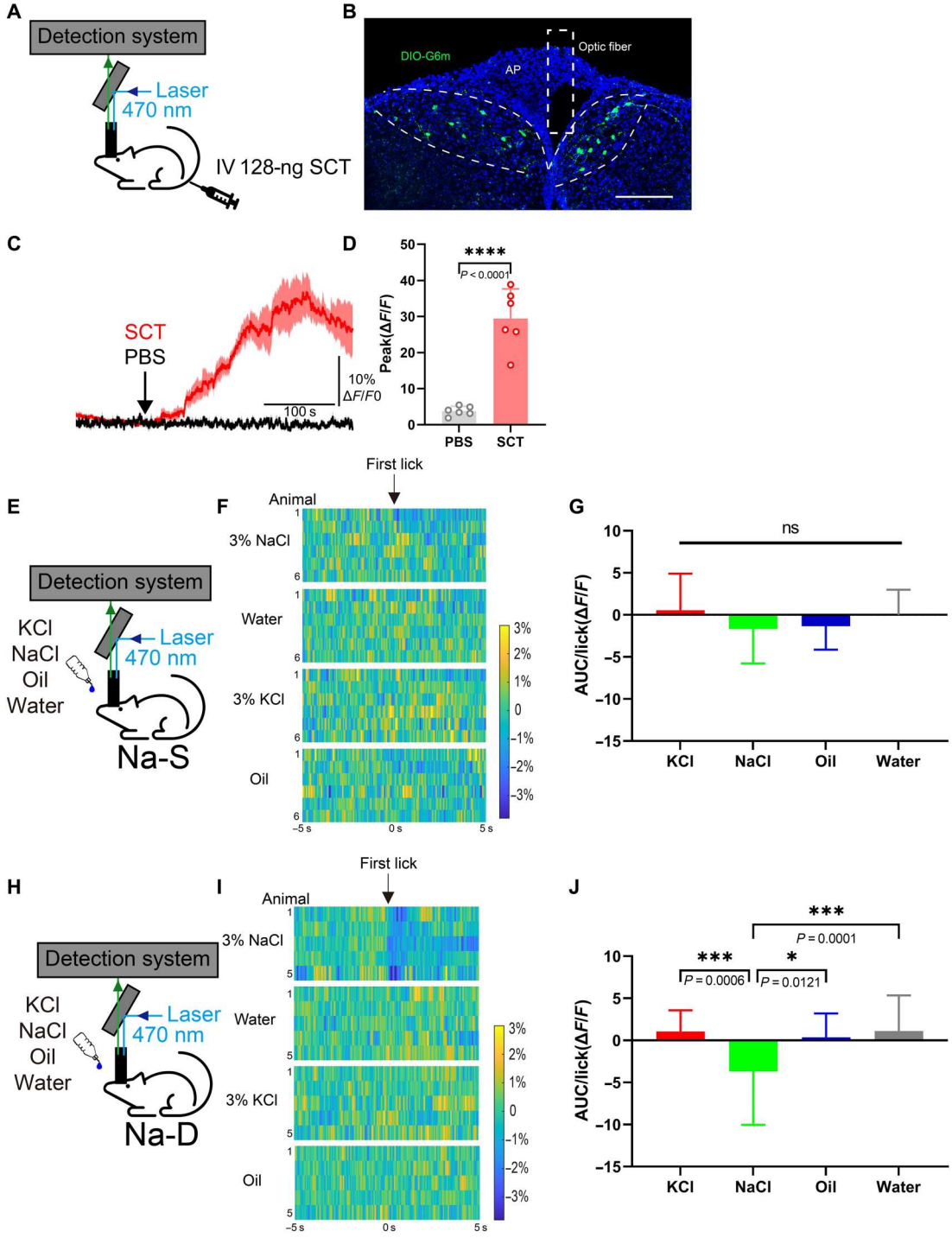

Fig. 5. NTS-SCTR$^+$ neurons presented neural activity associated with sodium appetite. (**A** and **B**) Schematic of fiber photometry recording under IV-SCT injection. Scale bar, 200 μm. (**C**) Representative calcium peak image showing the effect of IV-SCT or PBS on NTS neuronal activities. A total of 7-min traces were recorded, including 2 min before and 5 min after injection. $n = 6$ trials from six mice in each group. (**D**) Peak values of calcium transients were significantly elevated with SCT injection. Unpaired Student's t test, $t = 7.586$. $n = 6$ mice in each group. (**E**) Schematic of fiber photometry recording for water, NaCl, KCl, and oil intake under Na-S. (**F**) Heatmap of calcium signal changes of NTS neurons. A total time of 10 s was recorded, including 5 s before and 5 s after licking behaviors. For each scenario, a total of 30 traces from six mice were recorded and analyzed, and the signal strengths were averaged for each animal. (**G**) Quantification of area under the curve (AUC) of calcium signal showing that neuron activities remained unchanged under Na-S. One-way ANOVA, $F_{3,128} = 2.807$. (**H**) Schematic of fiber photometry recording for water, NaCl, KCl, and oil intake under Na-D. (**I**) Heatmap of calcium signal changes of NTS neurons. A total time of 10 s was recorded, including 5 s before and 5 s after licking behaviors. For each scenario, a total of 34 traces from five mice were recorded and analyzed, and the signal strengths were averaged for each animal. (**J**) Quantification of AUC of showing that neuron activities were depressed after saline intake under Na-D. *$P < 0.05$, **$P < 0.01$, ***$P < 0.001$, and ****$P < 0.0001$, with significant difference. All data were presented as means ± SD.

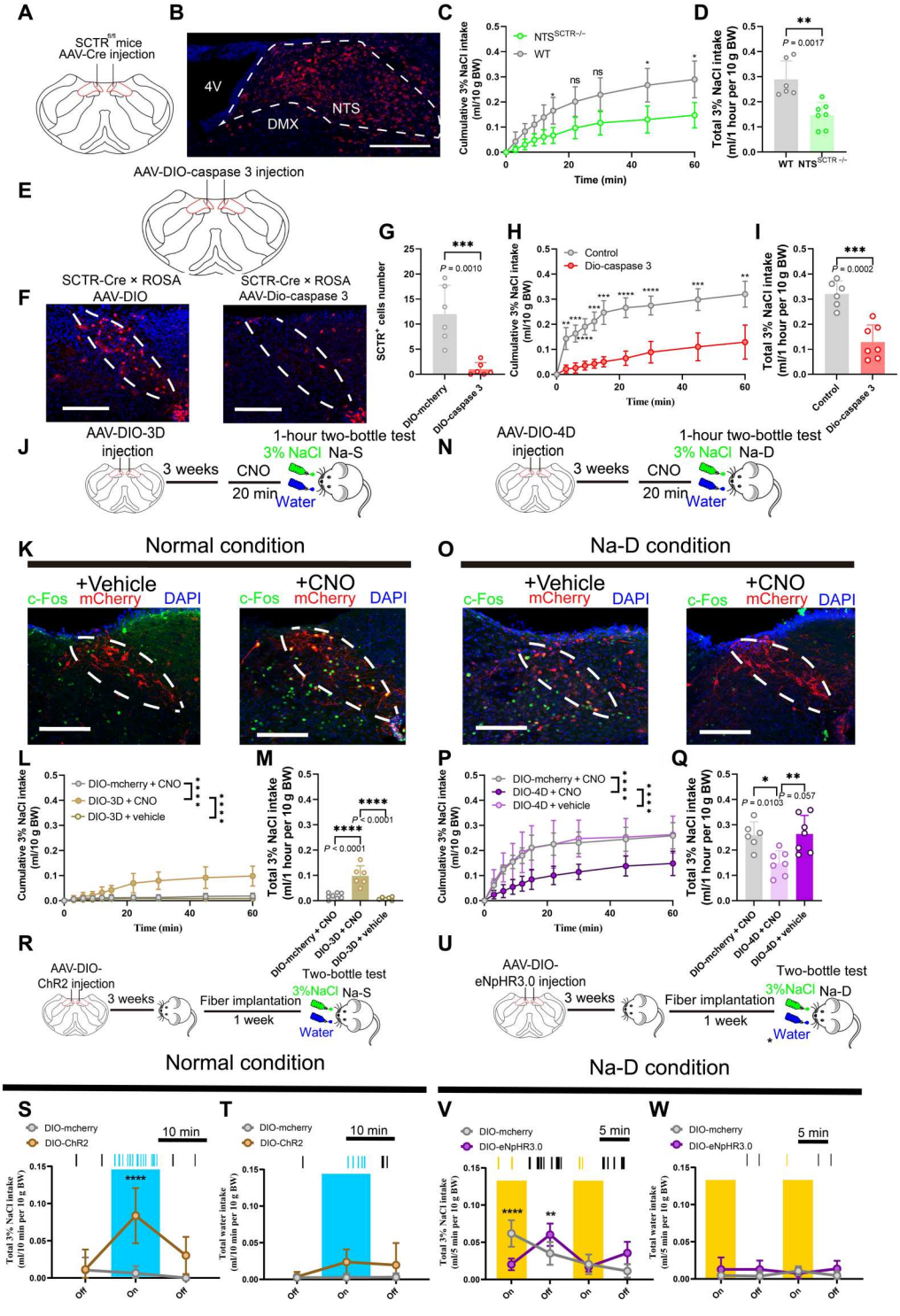

Fig. 6. NTS-SCTR$^+$ neurons are necessary for driving salt intake. (**A** and **B**) Virus injection into the NTS. Scale bar, 200 μm. (**C** and **D**) Cumulative saline intake (C) and total volume (D) in the NTS-SCTR KD under Na-D. Two-way ANOVA, group factor $F_{1,11} = 18.43$; unpaired Student's *t* test, $t = 4.130$. $n = 7$ mice in each group. (**E** to **G**) Ablation of SCTR$^+$ cells in the NTS. $t = 4.593$. $n = 6$ mice in each group. Scale bars, 200 μm. (**H** and **I**) Cumulative saline intake (H) and total volume (I) under NTS-SCTR$^+$ neuron ablation. Two-way ANOVA, group factor $F_{1,16} = 101.1$; unpaired Student's *t* test, $t = 5.631$. $n = 6$ and 7 mice in control and DIO-Caspase 3 group, respectively. (**J** and **K**) Chemogenetic activation of NTS-SCTR$^+$ neurons under Na-S. Scale bars, 200 μm. (**L** and **M**) Cumulative saline intake (L) and total volume (M) after CNO injection. Two-way ANOVA, group factor $F_{2,170} = 108.2$; one-way ANOVA, $F_{2,17} = 7.553$. $n = 8$, 6, and 8 mice in control, DIO-3D + CNO, and DIO-3D group, respectively. (**N** and **O**) Chemogenetic inhibition of NTS-SCTR$^+$ neurons under Na-D. Scale bars, 200 μm. (**P** and **Q**) Cumulative saline intake (P) and total volume (Q) after CNO injection. Two-way ANOVA, group factor $F_{2,170} = 80.64$; one-way ANOVA, $F_{2,17} = 1.135$. $n = 6$, 7, and 6 mice in control, DIO-4D + CNO, and DIO-4D group, respectively. (**R** to **T**) Optogenetic activation of the NTS-SCTR$^+$ neurons under Na-S–triggered saline (S) but not water (T) intake under Na-S condition. Two-way ANOVA, group factor $F_{1,48} = 34.33$; $n = 9$ mice in each group. (**U** to **W**) Optogenetic inhibition of the NTS-SCTR$^+$ neurons under Na-D–depressed saline (V) but not water (W) intake under Na-D conditions. Two-way ANOVA, group factor $F_{1,40} = 13.48$; $n = 6$ mice in each group. *$P < 0.05$, **$P < 0.01$, ***$P < 0.001$, and ****$P < 0.0001$, with significant difference. All data were presented as means ± SD.

light-stimulated facilitation or inhibition of saline intake was instantly induced and was rapidly lifted when the light was removed. In an alternative approach, the light activation of NTS-SCTR$^+$ neurons directed a conditional place preference for saline chamber in Na-S mice (fig. S10). Since the heat rate rhythm was unaffected by such light stimulation (fig. S11), these results supported the involvement of NTS-SCTR$^+$ neurons in specifically regulating salt drinking behaviors.

Subsequently, we analyzed the anatomical features of these NTS-SCTR$^+$ cells in the context of sodium appetite regulation. As these cells did not belong to previously established HSD2$^+$ neurons (Fig. 7, A and B) and did not innervate these HSD2$^+$ cells (fig. S12), we propose that they may have distinct circuitry connections.

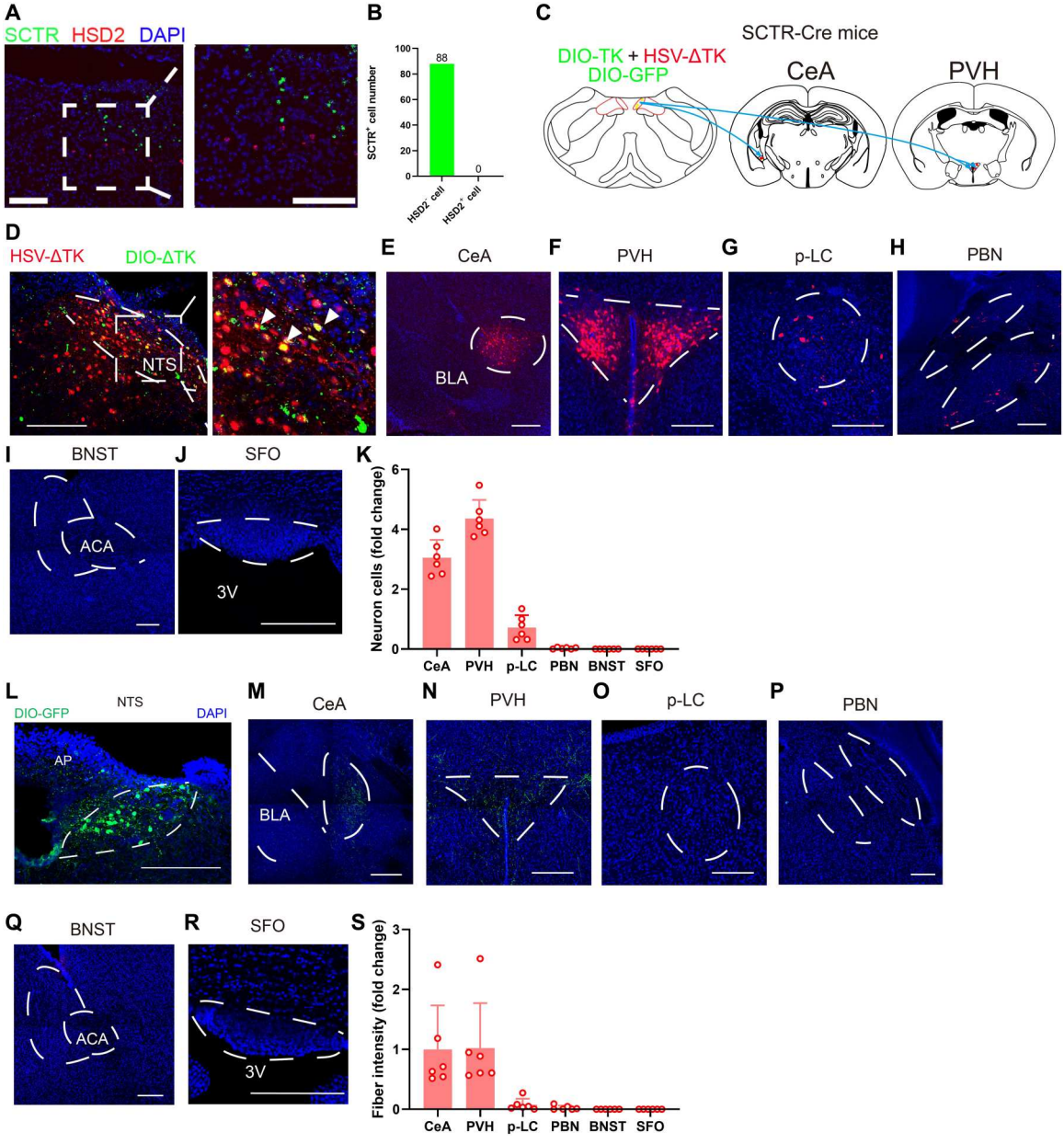

Fig. 7. NTS-SCTR$^+$ neurons preferentially project to PVH nuclei. (**A**) Representative RNAscope images showing that SCTR$^+$ cells are not HSD2$^+$ cells. Scale bars, 200 μm. (**B**) Quantification of HSD2$^+$ neurons showed their minimal overlapping with SCTR$^+$ neurons in the NTS. $n = 88$ neurons from three mice. (**C**) Schematic diagram showing the transsynaptic anterograde labeling. (**D** to **J**) Confocal images of DIO-ΔTK and HSV showing downstream nuclei from SCTR$^+$ neurons in the NTS. Scale bars, 200 μm. (**K**) Quantification of downstream nuclei from SCTR$^+$ neurons in the NTS. Means ± SD. (**L** to **R**) Confocal images of DIO-GFP showing projecting terminus from SCTR$^+$ neurons in the NTS. Scale bars, 200 μm. (**S**) Quantification of fiber fluorescence of projecting terminus from SCTR$^+$ neurons in the NTS. *$P < 0.05$, **$P < 0.01$, ***$P < 0.001$, and ****$P < 0.0001$, with significant difference.

Using an anterograde transsynaptic strategy by co-infecting AAV-DIO-TK and HSV-△TK or DIO-GFP into the NTS of SCTR-Cre mice (Fig. 7C), we selectively traced the downstream target of NTS-SCTR$^+$ cells (Fig. 7D). These cells mainly project to PVH and CeA, in addition to the limited terminus within the p-LC and PBN, and no projection was found in the SFO or BNST (Fig. 7, E to K). As an alternative approach, the axonal terminal fibers were labeled by AAV-DIO-GFP (Fig. 7L), which further confirmed the projection of NTS-SCTR$^+$ neurons to PVH and CeA (Fig. 7, M to S). In specific, NTS-SCTR$^+$ cells selectively innervated MC4R$^+$ neurons, but no VP$^+$ or OCT$^+$ cells in PVH (fig. S13), implying its unique physiological functions via downstream projections.

Last, we compared the modulatory effect of the NTS^{SCTR+}→PVH or CeA circuit on salt intake by local light activation or inhibition of the NTS-SCTR$^+$ terminus during the two-bottle assay (Fig. 8, A and B). Under Na-S conditions, light activation of the NTS^{SCTR+}→PVH pathway rapidly potentiated saline intake (Fig. 8C) but left the total water volume unchanged

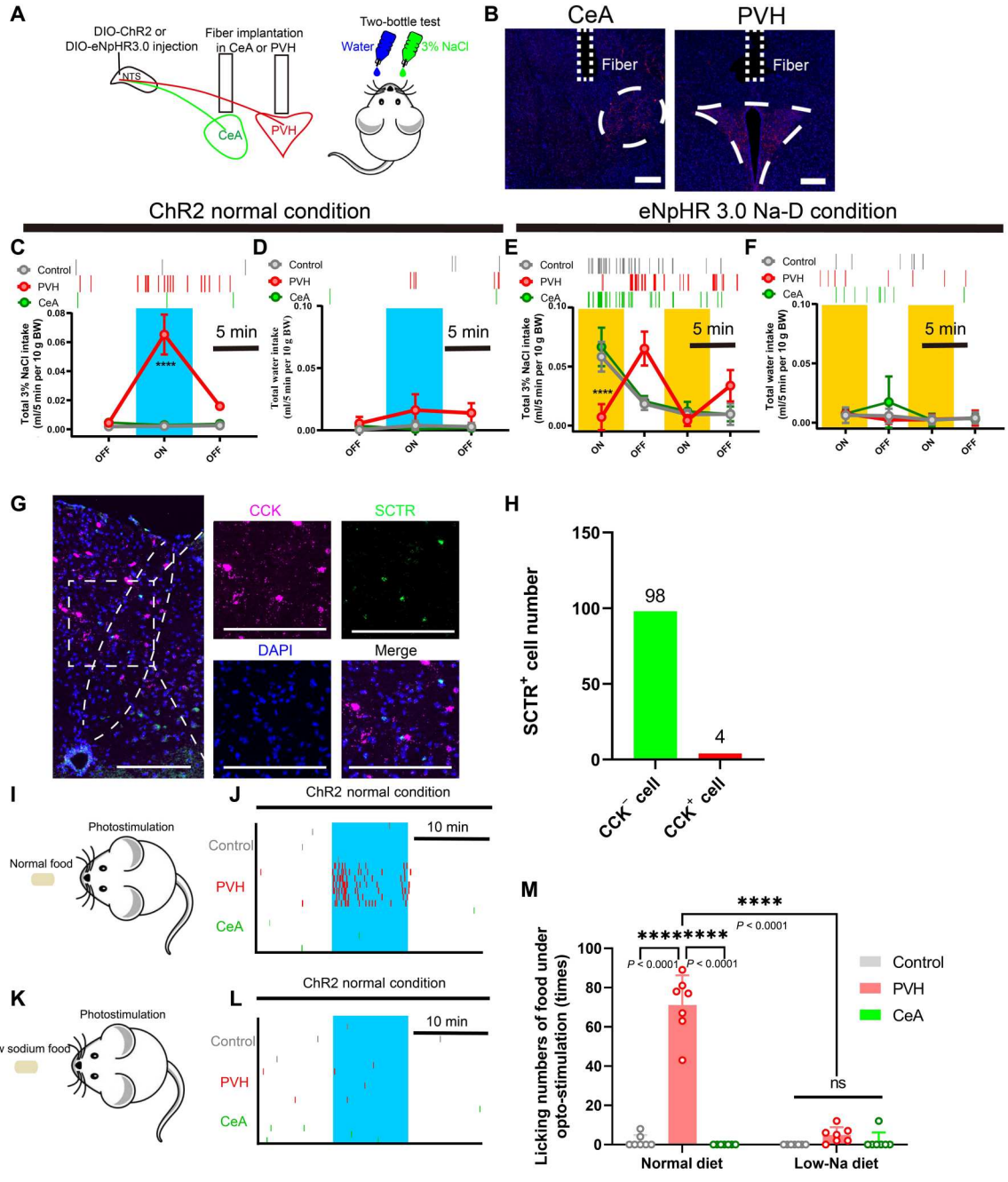

Fig. 8. NTS-SCTR$^+$ neurons specifically facilitate sodium appetite by projecting to PVH. (**A** and **B**) Schematic diagram of the optogenetic setup for activating NTS-SCTR$^+$ neuronal terminals in CeA or PVH. Scale bars, 200 μm. (**C** and **D**) Activating NTS-SCTR$^+$ terminals in PVH, but not CeA, triggers sodium intake under Na-S conditions. Two-way ANOVA, group factor $F_{2,42} = 34.36$; $n = 5$ in each group. (**E** and **F**) Optogenetic inhibition of NTS-SCTR$^+$ terminals in PVH, but not CeA, abolished sodium intake in Na-D mice. Two-way ANOVA, group factor $F_{2,52} = 42.01$; $n = 5$ in each group. (**G**) Representative RNAscope image showing that SCTR$^+$ cells are not CCK$^+$ cells. Scale bars, 200 μm. (**H**) Quantification of CCK$^+$ neurons overlapping with SCTR$^+$ neurons in the NTS. $n = 106$ cells from 3 mice. (**I** and **J**) Activating NTS-SCTR$^+$ terminals in PVH, but not CeA, induced the intake of 0.5% Na–containing food. A total of seven trials were extracted from five mice. (**K** and **L**) Activating NTS-SCTR$^+$ terminals in PVH and CeA did not alter the intake of low-Na food. A total of seven trials were extracted from five mice. (**M**) Activating NTS-SCTR$^+$ terminals in PVH, but not CeA, triggers the intake of normal diet, but not low-Na diet under Na-S. Two-way ANOVA, group factor $F_{2,36} = 140.2$; a total of seven trials were extracted from 5 mice. *$P < 0.05$, **$P < 0.01$, ***$P < 0.001$, and ****$P < 0.0001$, with significant difference. All data were presented as means ± SD.

(Fig. 8D). In Na-D mice, light inhibition of the PVH terminus strongly abolished salt appetite (Fig. 8E) but did not affect water intake (Fig. 8F). The manipulation of CeA, however, did not change either saline or water intake in these animals (Fig. 8, C to F). These results converged to support that the NTS $^{SCTR+}$→PVH pathway was necessary for eliciting salt intake via monosynaptic excitatory transmission (fig. S14). Since cholecystokinin-positive (CCK^+) cells in the NTS also project to PVH to inhibit food intake (*37*, *38*), we further analyzed such possibly confounding factors. The first piece of evidence came from the fact that only minimal (3.9%) overlapping existed between $SCTR^+$ and CCK^+ in NTS cells (Fig. 8, G and H). Second, the light activation of the NTS^{SCTR+}→PVH pathway triggered food intake toward normal diet (Fig. 8, I and J) but not low-sodium chows under Na-D conditions (Fig. 8, K to M). In summary, NTS-$SCTR^+$ neurons promote sodium intake but not the appetite for food or water, specifically via their excitatory projections to PVH (fig. S15).

DISCUSSION

Sophisticated neural and endocrine pathways are critical for sodium homeostasis, while the potential linkage between peripheral hormonal factors and neural circuits remains unclear. In this study, we demonstrated a previously unrecognized pathway by which colon SCT responds to sodium depletion and centrally facilitates salt intake. Although the role of ANG II and aldosterone has been appreciated in regulating salt homeostasis in renal tissues (*6*–*8*) and in the brain (*10*, *11*), our work provides a complete peripheral-central axis in mediating salt homeostasis. Of note, because of the relatively short half-life of circulating SCT (*39*), this neuropeptide pathway confers higher flexibility to regulate salt appetite in response to body sodium status.

Classical views agree that sodium intake is tightly mediated by ANG II and aldosterone systems. In addition to the peripheral effect in driving kidney sodium reabsorption in the renal distal nephron via epithelial sodium channel (ENaC) (*9*), the ANG II pathway also induces salt intake via an SFO→spBNST circuit (*10*). Similar to ANG II, aldosterone in the brain can induce sodium appetite (*40*, *41*) via NTS-$HSD2^+$ neurons that can project to the p-LC (*14*), PBN (*3*), and BNST (*1*). The current study, on the other hand, identified an NTS-$SCTR^+$ neuronal subpopulation that is distinct from $HSD2^+$ cells in terms of unique projecting patterns. Moreover, since $SCTR^+$ neurons did not connect with $HSD2^+$ cells, these two subpopulations of NTS neurons may have distinct physiological functions. Our findings thus expand the knowledge of the central homeostatic regulation of salt intake and provide more targets for correcting body sodium imbalance.

As the regulatory center for vital physiological functions, NTS regulates salt homeostasis due to its sensitivity to hormonal factors and projections to different downstream targets (*1*, *3*, *42*). In vitro autoradiographic SCT incubation showed that the NTS had the highest SCT binding affinity (*43*), and SCT can depolarize NTS neurons by activating a nonselective cationic conductance (*44*). These results indicated possible roles of SCT in mediating salt homeostasis within the NTS. Here, we generated an SCTR-Cre;ROSA-tdTomato reporter line and reported the spatial expressional profile of SCTR at single-cell resolution. The spNTS had the highest SCTR expression level, followed by AP, while BNST, p-LC, PBN, SFO, and PVH only showed limited SCTR expression. The transcriptional pattern of SCTR among the major nuclei of salt homeostasis indicated that NTS might be the primary target of SCT. Consistent with a previous study (*44*), NTS-$SCTR^+$ cells can be activated by peripheral SCT to drive salt intake under Na-D. Furthermore, sodium intake was decreased in NTS-specific SCTR gene KD mice, and manipulation of NTS-$SCTR^+$ neurons could trigger saline drinking episodes even in Na-S mice. These results highlighted the central role of SCT in modulating NTS neurons to facilitate sodium intake.

Two subpopulations of NTS neurons have been previously characterized, including $HSD2^+$ cells projecting to the p-LC, PBN, and BNST and CCK^+ neurons innervating CeA (*37*), PBN (*45*), and PVH (*38*). In the current study, the major downstream targets of $SCTR^+$ cells were located in PVH and CeA, whereas optogenetic manipulation showed that only the NTS→PVH pathway regulated sodium intake but not food or water appetite. Previous studies have shown that PVH plays a critical role in water and salt homeostasis, as lesions of PVH result in the abortion of the water drinking response (*46*), while CeA is related with licking behaviors (*47*). PVH also receives projections from the circumventricular organs (CVOs), leading to the release of vasopressin that can induce water reabsorption (*48*). Moreover, PVH neurons represent the primary source of oxytocin in the brain (*49*), and the central oxytocinergic pathway inhibits sodium intake (*50*). The current model in which PVH neurons receive signals from NTS-$SCTR^+$ cells to enhance sodium appetite provides further inputs for hypothalamic-driven salt appetite.

As one GI hormone, SCT is more prominently recognized due to its pleiotropic functions in the GI tract (*51*). In the small intestine, SCT could bind to SCTR in the intestinal vagal afferents and transmit signals to the hypothalamus to inhibit gastric acid secretion (*52*). In duodenum, the classical function of SCT is to stimulate pancreatic secretion in a response to the incoming acid chyme (*53*). In kidney, SCT was found to regulate renal water reabsorption (*54*). The role of SCT in water and salt homeostasis has been investigated in recent years. For example, SCT can trigger vasopressin release to compensate for water loss (*55*) and to induce aldosterone release in primary ZG cells (*56*, *57*). ANG II–induced water drinking behavior was attenuated in SCT or SCTR knockout mice (*58*). These studies indicate that SCT is involved in water and salt homeostasis in peripheral tissues. Within the brain, widely distributed SCTR (*59*, *60*) plus the BBB permeability of SCT (*24*, *61*) converged to indicate the potential role of peripheral SCT in centrally mediating water and salt homeostasis, the latter of which has been demonstrated in the current work. Nevertheless, our results did not exclude the possibility of colon SCT mediating renal reabsorption of sodium ions as previously recognized. Instead, SCT may have dual roles consisting of neural regulation for salt intake and renal sodium retention.

The mechanism by which colon tissue senses sodium levels and releases SCT remains as an interesting issue. In mammals, sodium channels in the tongue, kidney, and GI tract have dual functions, including sodium sensing and absorption (*62*). Although multiple segments of the digestive tract can absorb sodium ions (*63*, *64*), the increased SCT level is only observed in the colon under sodium depletion. The molecular mechanism for SCT release in colon tissues has not been completely resolved but may be related to the homeostatic regulation of membrane sodium channels. It is known that sodium imbalance leads to substantial changes in ENaC expression,

which plays a vital role in sodium acquisition in the colon (*62*). Furthermore, amiloride-induced blockage of the sodium channel leads to elevated blood aldosterone, supporting the potential role of the colon in sensing sodium level changes (*65*). Future studies can thus be performed to investigate the dynamics and trafficking of sodium channels in colon endocrine cells, to better correlate body sodium levels and SCT release. Our results also have potential values in clinical fields, as ileostomy patients showed chronic salt and water disorders, together with low urinary sodium excretion, all of which are similar to the mice after furosemide injection (*66*, *67*). Such clinical observations can be replicated in animal models, as previous studies indicated that SCT expression increased within 24 hours after colectomy and decreased significantly on day 14 in rats (*68*). Although no direct evidence has been provided for the role of colon SCT in sodium homeostasis in human patients, these studies did imply its possible involvement. Further works can be performed to explore the possibility of targeting SCT-SCTR for correcting sodium imbalance in colectomy patients.

In summary, the current study demonstrated a gut-brain pathway in which colon tissues respond to body sodium deficiency to produce SCT, which enters the brain to stimulate salt intake via an NTS^{SCTR+}→PVH circuit. Our results provide more insights for understanding the homeostatic control of sodium intake and provide previously unidentified targets for correcting body sodium imbalance.

MATERIALS AND METHODS

Experimental animals

Animal care and handling procedures were under the protocols approved by the Committee on the Use of Live Animals in Teaching and Research (CULATR) of the University of Hong Kong and the Ethics Committee of Experimental Animals of Jinan University. Mice used for the behavioral test were at least 6 weeks old with ~20 g body weight. Both males and females were used in this study. $SCT^{-/-}$ and $SCTR^{-/-}$ mice were generated by our group as previously documented (*31*). The SCTR-Cre transgenic mouse line was generated by inserting an IRES-iCre construct after the 14th exon of SCTR coding region (fig. S3). C57BL/6N mice were purchased from the University of Hong Kong. All mice were housed in a temperature-controlled room with a 12:12-hour light-dark cycle and were fed with water and low-sodium diet (0.01% Na, D02051701, Research Diets Inc.) or standard rodent chow (0.4 to 0.6% Na; TestDiet, no.5881) ad libitum.

Stereotaxic injection

Mice were anesthetized with ketamine (100 mg/kg) and xylazine (10 mg/kg), with removal of the hair by clipper and depilatory cream (VEET), and were fixed in a stereotaxic instrument (RWD, China) on a heating pad at 37°C. The scalp was incised to remove the muscle on the occipital bone for exposing the surgical site. The injection site was located, followed by muscle removal and microdrilling at the skull above. The coordinate of NTS was 7 mm along the AP axis, ±0.5 mm on the medial-dorsal (ML) axis, and 4.95 mm dorsal-ventral (DV) depth, with respect to bregma. Virus injection was performed with glass pipettes (WPI, #504949) connected to a nanoliter-volume injection pump with an intuitive SMARTouch controller (WPI, USA) at 60 nl/min. A total of 150-nl viral dilution was slowly injected into NTS. The glass pipette was placed in the NTS for 5 min before retraction. Mice were housed for 7-day recovery after surgery, and behavior tests were performed at 3 weeks after surgery.

For anterograde tracing, 150 nl of AAV2/9-Ef1α-DIO-EGFP-2A-TK-WPRE-pA was injected into the NTS. Another dosage of 150 nl of HSV-ΔTK-hUbC-tdTomato was injected into the NTS after 3 weeks. The mice were sacrificed 4 days later.

Vagotomy and intestinal viral injection

Mice were anesthetized with a mixture of ketamine and xylazine as described and fixed. Peritoneum and skin were incised to the exposed colon. Excision of the intestinal vague nerve is performed with sterile cotton swabs to retract the liver, and two glass pipettes to hold the esophagus and cut a 1- to 2-mm section off the intestinal vague nerve, followed by single house treatment for recovery. For viral transfection into colon tissues, a total of 100 μl of virus was injected in five different positions in the colon using an insulin needle. For each position, cotton swab was used for gently wiping of colon tissue to remove the connective tissue. A fine-needle was inserted horizontally into the colon which was hold by the forceps. . The needle was visible before injection, and after injection, a bubble could be found in the injection site. To validate the efficiency of vagotomy, intraperitoneal (IP) injection of WGA conjugated was performed.

Optic fiber implantation and optogenetic manipulation

AAV-DIO-ChR2 and AAV-DIO-eNpHR3.0 were injected into NTS of SCTR-Cre mice. Fiber implantation for optogenetic stimulation was also performed 3 weeks after viral injection. In brief, the scalp was incised, and the muscle was removed by forceps to expose the skull. A microdrill was used to make a small hole, and a customized optic fiber (1.25 mm diameter for optogenetic and 2.5 mm for fiber photometry, ThinkerTech) was inserted. Dental cement and two bone screw (RWD, China) were performed to fixation. Mice were singly housed for 1-week recovery. The coordinates are as follows: −7 mm (AP), 0 mm (ML), and −4.9 mm (DV) for NTS; −0.8 mm (AP), 0.1 mm (ML), and −4.5 mm (DV) for PVH; and −1.45 mm (AP), ±2.8 mm (ML), and −4.75 mm (DV). Mice were housed in an acrylic cage 24 hours before the behavior test. For photo-inhibition, after furosemide injection, no-sodium diet was provided for 24 hours.

Implantation of osmotic pump

Osmotic pump (2002 W, RWD, China) with capsule carrying 200 μl of SCT antibody (0.01 mg/ml; bs-0088R, Bioss, USA) was fixed beneath the back skin. A plastic cannula was inserted into the ventricle, and the osmotic pump was connected. Data were collected 1 week after recovery.

Two-bottle assay

A single dosage of furosemide (50 mg/kg) and 24-hour no-sodium diet were applied to make sodium deficiency condition. Blood serums were collected for measuring plasma Na^+ assay with an assay kit (E-BC-K207-S, Elabscience). All animals were pretrained before formal experiments to be familiar with the water bottle. Mice under Na-D condition need to have obvious licking behavior in 30 min after being accessible to the water and sodium bottle during training. Mice were housed in acrylic boxes 1 day before the behavior test. Na-D and Na-S mice were kept in an acrylic box for 1 hour

with two bottles containing water and 3% NaCl, respectively. The bottle consisted of a needle tubing in the end of a 2-ml pipette with a clear scale to record the liquid layer. If there is air column in the fore-end of the 2-ml pipette, the plunger rod was slowly rotated until the column disappears. If there are too many air bubbles in the 2-ml pipette and the bubbles are unmeasurable, the data will be abandoned. The trails with many irregular bubbles in the middle of the pipette that lead to inaccurate data were not accounted for. The water and salt intake were continuously monitored for 60 min. For ChR2-mediated photostimulation, mice were freely accessible to water and 3% NaCl for 30 min, and laser pulse was delivered from 10 to 20 min. For eNpHR3.0-directed photoinhibition, laser pulse was given during 0 to 5 min and 10 to 15 min.

Peripheral drug injection

IV injection of SCT (8, 32, and 128 ng) and SCT5-27 (1.5 μg) was performed before two-bottle behavior tests. CNO (25 mg/kg) was IP injected 20 min before behavior test of chemo-genetics. For WGA IP injection, 200 μg of WGA, Alexa Fluor 555 conjugate (W32464, Thermo Fisher Scientific) was injected into each mouse, and the mice were sacrificed 3 days later.

Ex vivo electrophysiological recording

SCTR-Cre;ROSA-tdTomato mice were anesthetized with isoflurane and perfused with ice-cold artificial CSF (aCSF). VT1000S Vibratome (Leica Microsystems, Wetzlar, Germany) was used for preparing coronal NTS slices (270 μm thickness), which were recovered in an ice-cold, oxygenated (95% O_2 and 5% CO_2) aCSF (126 mM NaCl; 2.5 mM KCl, 1.2 mM NaH_2PO_4, 10 mM glucose, 26 mM $NaHCO_3$, 2.4 mM $CaCl_2$ and 1.2 mM $MgCl_2$, and 295 mOsm, at pH 7.4) bath. Warmed (~33.5°C) aCSF was used to incubate brain slices for 25 min, and the slices were placed at room temperature for recovery at 30 min before recording. Filamented borosilicate glass capillary tubes (inner diameter, 0.86 μm) were drawn by a horizontal pipette puller (PC-100, Narishige) to make recoding electrodes. With resistance ranging from 4.5 to 6 megohms, the pipettes were filled with intracellular solution (135 mM K-gluconate, 5 mM KCl, 10 mM Hepes, 0.2 mM EGTA, 4 mM MgATP, 10 mM Na_2-phosphocreatine, and 0.3 mM Na_3GTP; pH was adjusted to 7.4 with KOH).

To measure the effect of SCT on NTS-SCTR$^+$ neuron, a depolarizing current (0.8-s stimulation for each trace from 0 to 80 pA) was applied. Action potentials (APs) from one cell were recorded before and 9 min after 400 nM SCT incubation. The membrane potential was held at −60 mV.

To validate the efficiency of ChR2 or eNpHR3.0, whole-cell current clamp recording was performed. The optic excitation spikes were measured with 473-nm light pulses (20 Hz, 5-ms duration). The optic inhibition AP induced by eNpHR3.0 was recorded by 594-nm light stimulation (20 mW, 1-s pulse duration).

Evoked postsynaptic currents were recorded by 473-nm light stimulation (5-ms duration) at axonal terminals of NTS-SCTR$^+$ neurons transfected with ChR2 in PVH. Brain slices were perfused with tetrodotoxin (1 μM) followed by 4-aminopyridine (100 μM) to confirm the monosynaptic connections from NTS-SCTR$^+$ neurons to PVH. The membrane potential was held at −65 mV during recording.

Cell membrane potentials were recorded at 10 kHz, and traces were low pass–filtered at 2 kHz. All recordings were performed using a Multiclamp 700B amplifier (Molecular Devices, USA), and light pulses were transmitted through digital commands from Digidata 1550A. Series resistance (Rs) was kept within 25 megohms and monitored throughout the experiments. The data were excluded when Rs changed >20% during recording. Clampfit 10.0 software (Molecular Devices, USA) was used for data analysis.

In vivo fiber photometry

AAV2/9-hSyn-DIO-GCaMP6m was transfected into NTS of SCTR-Cre mice at 3 weeks before optic fiber implantation as described above. During photometric recording, a dichroic mirror (Edmund Optics) focused through an objective lens [20×; numerical aperture (NA), 0.4; Olympus, Japan] was used to reflect light-emitting diode (405-nm Lumileds, 470-nm LUXEON Rebel, and 572-nm LUXEON Rebel). An optical fiber (200 nm outside diameter, NA = 0.37) was used for guiding the light. The laser power was maintained within 40 to 60 μW. The fluorescence signals from the optical fiber were filtered (87753, Edmund Optics) and integrated by a photomultiplier tube (H10721, Hamamatsu). An amplifier and a low-pass filter (35-Hz cutoff, ThinkerTech) converted the photomultiplier tube current output to voltage. MATLAB-based photometry software (ThinkerTech, China) was used for digitalizing the analog voltage signals at 100 Hz. Before the experiment, the optic was bleached for at least 1 hour to avoid autofluorescence. Mice were provided with low-sodium diet and housed in acrylic cages 1 day before fiber recording.

Fluorescent staining

Mice were anesthetized and perfused with 30 ml of phosphate-buffered saline (PBS), followed by 30 ml of 4% paraformaldehyde (PFA; Biosharp, 71010900). The brains were kept in 4% PFA at 4°C overnight, followed by 30% sucrose for 24 hours. The sample was embedded in OCT (Sakura, 4583) for at most 1 week before sectioning. For the immunofluorescence experiment, 30-μm brain sections were incubated at 0.3% Triton X-100 in CAS-Block (Life Technologies, 2354658) for 2 hours. Sections were then incubated for 24 hours with primary antibodies diluted in blocking buffer with 0.3% Triton X-100: sheep anti-TPH (1:500, Millipore, AB1541), vimentin XP rabbit monoclonal antibody (Alexa Fluor 48 conjugate) (1:400, Cell Signaling, 9854), guinea pig anti–c-Fos (1:500, Synaptic Systems, 226005), rabbit anti-MC4R (1:1000, Abcam, ab24233), rabbit anti-oxytocin (1:10,000, Immunostar, AB_572258), rabbit anti-vasopressin (1:1000, Millipore, AB1565), rabbit anti-HSD11B2 (1:500, Proteintech, 14192-1-AP), rabbit anti-mcherry antibody (DsRed) (1:500, Clontech, Mountain View, CA), and anti-GFP antibody (1:500, Aves Labs, GFP-1020). Cells were washed with PBS five times, and then sections were incubated in secondary antibodies for 2 hours: donkey anti-sheep immunoglobulin G (IgG) H&L (Alexa Fluor 488) (Abcam, ab150177), goat anti–guinea pig IgG (H+L) highly cross-adsorbed secondary antibody, Alexa Fluor 488 (Invitrogen, A-11073), Alexa Fluor 680 goat anti-rabbit IgG (H+L) (1:500, Invitrogen, A21109), Alexa Fluor 594 donkey anti-rabbit IgG (H+L) (1:500, Invitrogen, A21207), and Alexa Fluor 488 goat anti-chicken IgG (H+L) (1:500, Invitrogen, A11039). Double staining of SCTR/c-Fos was performed by fluorescence in situ hybridization (FISH) following the manufacturer's instructions of a PinpoRNA Multiplex Fluorescent RNA In Situ

Hybridization kit (Pinpoease). Double staining of SCTR/Vglut2 and double staining of SCTR/HSD2, SCTR/tdtomato, and SCTR/CCK were performed by FISH following the manufacturer's instructions of RNAscope multiplex fluorescent V2 assay (ACD).

Real-time qPCR

The small intestine, duodenum, kidney, and colon tissues were incubated in TRIzol and treated with an EZ-10 total RNA Mini-Preps kit (BBI, USA) overnight to isolate total RNA, which was reversely transcribed into complementary DNA by a PrimeScript RT reagent kit (Takara, Japan). TB green premix EX Taq II (Takara, Japan) was used for quantitative reverse transcription PCR (qRT-PCR). The peak of the melting curve was used. $\Delta\Delta C_q$ values after normalization to glyceraldehyde-3-phosphate dehydrogenase (GAPDH) was used to calculate relative expression level. Primers for RT-PCR (Sangon, China) include the following: *Sct*, AGACACTCAGACGGAATGT TCA (forward) and CTGGTCCTCTAAGGGCTTGGA (reverse); *Gapdh*, *AGGTCGGTGTGAACGGATTTG* (forward) and TGTAG ACCATGTAGTTGAGGTCA (reverse); *Tph1*, TTCTGACCTGGA CTTCTGCG (forward) and GGGGTCCCCATGTTTGTAGT (reverse); *Glp1*, GGCACATTCACCAGCGACTAC (forward) and CAATGGCGACTTCTTCTGGG (reverse); *Aqp1*, CAT CACCTCCTCCCTAGTCG (forward) and GCACAGTACCAGCT GCAGAG (reverse); *Aqp3*, GGGATTGTTTTTGGGCTGTA (forward) and CAGAGGGATAGGTGGCAAAG (reverse); *Aqp4*, CCTCATCTCCCTTTGCTTTG (forward) and GTGCACACCAT GGCTACAGT (reverse); and *Aqp8*, CCATTCTCCATTGGCTTC TC (forward) and CCAATGGAAGTCCCAGTAGC (reverse).

Enzyme-linked immunosorbent assay

Protein samples from the small intestine, duodenum, and colon were ultrasonically homogenized in radioimmunoprecipitation assay (RIPA) buffer containing protease inhibitor and phosphatase inhibitors. Tissue lysates were treated by 2000*g* centrifugation at 4°C for 12 min. The sample was kept at −80°C for further experiments. An SCT (mouse) ELISA kit (Phoenix Pharmaceuticals, USA) was used for quantification following the manual instruction. For CSF SCT concentration, a 30-gauge needle was used to collect CSF from the fourth ventricle. On average, 8 μl of CSF was collected from one mouse, and seven mice were pooled as a sample before ELISA.

Conditional place preference

To test conditional place preference, a 10 cm × 25 cm acrylic box was performed with two bottles containing 3% NaCl and water on two sides. Before conditioning on day 1, each mouse was placed separately in the acrylic box for 5 min, with free access to both bottles. The conditioning place preference was recorded in the next three continuous days. Light pulses (473 nm; 20 Hz, 5-ms pulse duration) were delivered during 0 to 5 min. Data were analyzed with behavior tracking software (TopScan).

Heart rate measurements

For ChR2 photostimulation, the heart rate of mice was continuously measured using a pulse oximeter, and then the number of beats was reported at 15-Hz intervals (MouseOxPlus Software; Starr Life Science) for head-fixed mice. Heart rate values ranged from 500 to 700 beats per minute. The mice were habituated to the sensor for at least 10 min. Light pulses (473 nm; 20 Hz, 5-ms pulse duration) were delivered during 10 to 70 s.

Statistical analysis

All data were shown as means ± SD. Prism 9.0 software (GraphPad Software, La Jolla, USA) was used for data analysis and figure plotting. Parametric datasets were compared using unpaired Student's *t* test. Mann-Whitney test was used for comparison between two groups of nonparametric data. One-way analysis of variance (ANOVA) and Kruskal-Wallis test were used for comparison among more than two groups, under parametric or nonparametric scenarios, respectively. Two-way ANOVA was adopted when two independent variables were co-considered, followed by a Sidak post hoc comparison.

Supplementary Materials

This PDF file includes:

Figs. S1 to S15
Table S1

View/request a protocol for this paper from *Bio-protocol*.

REFERENCES AND NOTES

1. J. M. Resch, H. Fenselau, J. C. Madara, C. Wu, J. N. Campbell, A. Lyubetskaya, B. A. Dawes, L. T. Tsai, M. M. Li, Y. Livneh, Q. Ke, P. M. Kang, G. Fejes-Tóth, A. Náray-Fejes-Tóth, J. C. Geerling, B. B. Lowell, Aldosterone-sensing neurons in the NTS exhibit state-dependent pacemaker activity and drive sodium appetite via synergy with angiotensin II signaling. *Neuron* **96**, 190–206. e7 (2017).
2. E. Watanabe, A. Fujikawa, H. Matsunaga, Y. Yasoshima, N. Sako, T. Yamamoto, C. Saegusa, M. Noda, Na_v2/NaG channel is involved in control of salt-intake behavior in the CNS. *J. Neurosci.* **20**, 7743–7751 (2000).
3. B. C. Jarvie, R. D. Palmiter, HSD2 neurons in the hindbrain drive sodium appetite. *Nat. Neurosci.* **20**, 167–169 (2017).
4. R. Weisinger, R. S. Weisinger, D. A. Denton, R. Di Nicolantonio, D. K. Hards, M. J. McKinley, B. Oldfield, P. G. Osborne, Subfornical organ lesion decreases sodium appetite in the sodium-depleted rat. *Brain Res.* **526**, 23–30 (1990).
5. S. Park, K. W. Williams, C. Liu, J.-W. Sohn, A neural basis for tonic suppression of sodium appetite. *Nat. Neurosci.* **23**, 423–432 (2020).
6. K. J. Catt, J. P. Harwood, G. Aguilera, M. L. Dufau, Hormonal regulation of peptide receptors and target cell responses. *Nature* **280**, 109–116 (1979).
7. G. Aguilera, K. Catt, Regulation of aldosterone secretion by the renin-angiotensin system during sodium restriction in rats. *Proc. Natl. Acad. Sci. U.S.A.* **75**, 4057–4061 (1978).
8. M. E. Raichle, R. L. Grubb Jr., Regulation of brain water permeability by centrally-released vasopressin. *Brain Res.* **143**, 191–194 (1978).
9. M. E. Briet, E. L. Schiffrin, Aldosterone: Effects on the kidney and cardiovascular system. *Nat. Rev. Nephrol.* **6**, 261–273 (2010).
10. T. Matsuda, T. Y. Hiyama, F. Niimura, T. Matsusaka, A. Fukamizu, K. Kobayashi, K. Kobayashi, M. Noda, Distinct neural mechanisms for the control of thirst and salt appetite in the subfornical organ. *Nat. Neurosci.* **20**, 230–241 (2017).
11. R. L. Thunhorst, D. A. Fitts, Peripheral angiotensin causes salt appetite in rats. *Am. J. Physiol.* **267**, R171–R177 (1994).
12. R. R. Sakai, S. Y. Chow, A. N. Epstein, Peripheral angiotensin II is not the cause of sodium appetite in the rat. *Appetite* **15**, 161–170 (1990).
13. M. Zhang, Y. Mao, S. H. Ramirez, R. F. Tuma, T. Chabrashvili, Angiotensin II induced cerebral microvascular inflammation and increased blood-brain barrier permeability via oxidative stress. *Neuroscience* **171**, 852–858 (2010).
14. S. Lee, V. Augustine, Y. Zhao, H. Ebisu, B. Ho, D. Kong, Y. Oka, Chemosensory modulation of neural circuits for sodium appetite. *Nature* **568**, 93–97 (2019).
15. J. C. Geerling, A. D. Loewy, Aldosterone-sensitive neurons in the nucleus of the solitary tract: Efferent projections. *J. Comp. Neurol.* **497**, 223–250 (2006).
16. J. C. Geerling, A. D. Loewy, Aldosterone in the brain. *Am. J. Physiol. Renal. Physiol.* **297**, F559–F576 (2009).
17. J. Funder, K. Myles, Exclusion of corticosterone from epithelial mineralocorticoid receptors is insufficient for selectivity of aldosterone action: In vivo binding studies. *Endocrinology* **137**, 5264–5268 (1996).
18. W. M. Pardridge, L. J. Mietus, Transport of steroid hormones through the rat blood-brain barrier: Primary role of albumin-bound hormone. *J. Clin. Invest.* **64**, 145–154 (1979).

19. L. S. Lara, R. Satou, C. R. T. Bourgeois, A. A. Gonzalez, A. Zsombok, M. C. Prieto, L. G. Navar, The sodium-activated sodium channel is expressed in the rat kidney thick ascending limb and collecting duct cells and is upregulated during high salt intake. *Am. J. Physiol. Renal. Physiol.* **303**, F105–F109 (2012).
20. J. Y. S. Chu, L. T. O. Lee, C. H. Lai, H. Vaudry, Y. S. Chan, W. H. Yung, B. K. C. Chowa, Secretin as a neurohypophysial factor regulating body water homeostasis. *Proc. Natl. Acad. Sci. U.S.A.* **106**, 15961–15966 (2009).
21. L. Zhang, B. K. C. Chow, The central mechanisms of secretin in regulating multiple behaviors. *Front. Endocrinol.* **5**, 77 (2014).
22. M. J. Lopez, B. H. Upchurch, G. Rindi, A. B. Leiter, Studies in transgenic mice reveal potential relationships between secretin-producing cells and other endocrine cell types. *J. Biol. Chem.* **270**, 885–891 (1995).
23. L. J. Billing, P. Larraufie, J. Lewis, A. Leiter, J. Li, B. Lam, G. S. H. Yeo, D. A. Goldspink, R. G. Kay, F. M. Gribble, F. Reimann, Single cell transcriptomic profiling of large intestinal enteroendocrine cells in mice–identification of selective stimuli for insulin-like peptide-5 and glucagon-like peptide-1 co-expressing cells. *Mol. Metab.* **29**, 158–169 (2019).
24. W. A. Banks, M. Goulet, J. R. Rusche, M. L. Niehoff, R. Boismenu, Differential transport of a secretin analog across the blood-brain and blood-cerebrospinal fluid barriers of the mouse. *J. Pharmacol. Exp. Ther.* **302**, 1062–1069 (2002).
25. R. F. Lundy Jr., M. Blair, N. Horvath, R. Norgren, Furosemide, sodium appetite, and ingestive behavior. *Physiol. Behav.* **78**, 449–458 (2003).
26. J. E. Jalowiec, Sodium appetite elicited by furosemide: Effects of differential dietary maintenance. *Behav. Biol.* **10**, 313–327 (1974).
27. J. F. Cryan, T. G. Dinan, Mind-altering microorganisms: The impact of the gut microbiota on brain and behaviour. *Nat. Rev. Neurosci.* **13**, 701–712 (2012).
28. D. Tomé, J. Schwarz, N. Darcel, G. Fromentin, Protein, amino acids, vagus nerve signaling, and the brain. *Am. J. Clin. Nutr.* **90**, 838S–843S (2009).
29. C. A. Zimmerman, E. L. Huey, J. S. Ahn, L. R. Beutler, C. L. Tan, S. Kosar, L. Bai, Y. Chen, T. V. Corpuz, L. Madisen, H. Zeng, Z. A. Knight, A gut-to-brain signal of fluid osmolarity controls thirst satiation. *Nature* **568**, 98–102 (2019).
30. T. Zhang, M. H. Perkins, H. Chang, W. Han, I. E. de Araujo, An inter-organ neural circuit for appetite suppression. *Cell* **185**, 2478–2494.e28 (2022).
31. R. Sekar, B. K. C. Chow, Secretin receptor-knockout mice are resistant to high-fat diet-induced obesity and exhibit impaired intestinal lipid absorption. *FASEB J.* **28**, 3494–3505 (2014).
32. L. Kennedy, H. Francis, P. Invernizzi, J. Venter, N. Wu, M. Carbone, M. Eric Gershwin, F. Bernuzzi, A. Franchitto, D. Alvaro, M. Marzioni, P. Onori, E. Gaudio, A. Sybenga, L. Fabris, F. Meng, S. Glaser, G. Alpini, Secretin/secretin receptor signaling mediates biliary damage and liver fibrosis in early-stage primary biliary cholangitis. *FASEB J.* **33**, 10269–10279 (2019).
33. A. S. KoPIN, M. B. Wheeler, A. B. Leiter, Secretin: Structure of the precursor and tissue distribution of the mRNA. *Proc. Natl. Acad. Sci. U.S.A.* **87**, 2299–2303 (1990).
34. J. M. Polak, I. Coulling, S. Bloom, A. G. Pearse, Immunofluorescent localization of secretin and enteroglucagon in human intestinal mucosa. *Scand. J. Gastroenterol.* **6**, 739–744 (1971).
35. N. Yanaihara, M. Sakagami, H. Sato, K. Yamamoto, T. Hashimoto, Immunological aspects of secretin. Substance P, and Vip. *Gastroenterology* **72**, 803–810 (1977).
36. J.-A. Wei, Q. Han, Z. Luo, L. Liu, J. Cui, J. Tan, B. K. C. Chow, K.-F. So, L. Zhang, Amygdala neural ensemble mediates mouse social investigation behaviors. *Natl. Sci. Rev.* , (2022).
37. O. Viltart, D. M. Sartor, A. J. M. Verberne, Chemical stimulation of visceral afferents activates medullary neurones projecting to the central amygdala and periaqueductal grey. *Brain Res. Bull.* **71**, 51–59 (2006).
38. G. D'Agostino, D. J. Lyons, C. Cristiano, L. K. Burke, J. C. Madara, J. N. Campbell, A. P. Garcia, B. B. Land, B. B. Lowell, R. J. Dileone, L. K. Heisler, Appetite controlled by a cholecystokinin nucleus of the solitary tract to hypothalamus neurocircuit. *ELife* **5**, e12225 (2016).
39. B. E. Kolts, J. E. McGuigan, Radioimmunoassay measurement of secretin half-life in man. *Gastroenterology* **72**, 55–60 (1977).
40. R. R. Sakai, B. S. Mcewen, S. J. Fluharty, L. Y. Ma, The amygdala: Site of genomic and nongenomic arousal of aldosterone-induced sodium intake. *Kidney Int.* **57**, 1337–1345 (2000).
41. H. Qiao, B. Hu, H. Zhou, J. Yan, R. Jia, B. Lu, B. Sun, X. Luo, Y. Fan, N. Wang, Aldosterone induces rapid sodium intake by a nongenomic mechanism in the nucleus tractus solitarius. *Sci. Rep.* **6**, 38631 (2016).
42. J. C. Geerling, A. D. Loewy, Aldosterone-sensitive neurons in the nucleus of the solitary tract: Bidirectional connections with the central nucleus of the amygdala. *J. Comp. Neurol.* **497**, 646–657 (2006).
43. S. Nozaki, R. Nakata, H. Mizuma, N. Nishimura, Y. Watanabe, R. Kohashi, Y. Watanabe, *In vitro* autoradiographic localization of ^{125}I-secretin receptor binding sites in rat brain. *Biochem. Biophys. Res. Commun.* **292**, 133–137 (2002).
44. B. Yang, M. Goulet, R. Boismenu, A. V. Ferguson, Secretin depolarizes nucleus tractus solitarius neurons through activation of a nonselective cationic conductance. *Am. J. Physiol. Regul. Integr. Comp. Physiol.* **286**, R927–R934 (2004).
45. C. W. Roman, V. A. Derkach, R. D. Palmiter, Genetically and functionally defined NTS to PBN brain circuits mediating anorexia. *Nat. Commun.* **7**, 11905 (2016).
46. M. B. Gutman, D. L. Jones, J. Ciriello, Effect of paraventricular nucleus lesions on drinking and pressor responses to ANG II. *Am. J. Physiol.* **255**, R882–R887 (1988).
47. D. Zheng, J.-Y. Fu, M.-Y. Tang, X.-D. Yu, Y. Zhu, C.-J. Shen, C.-Y. Li, S.-Z. Xie, S. Lin, M. Luo, X.-M. Li, A deep mesencephalic nucleus circuit regulates licking behavior. *Neurosci. Bull.* **38**, 565–575 (2022).
48. R. W. Lind, R. L. Thunhorst, A. K. Johnson, The subfornical organ and the integration of multiple factors in thirst. *Physiol. Behav.* **32**, 69–74 (1984).
49. G. J. De Vries, R. M. . Buijs, The origin of the vasopressinergic and oxytocinergic innervation of the rat brain with special reference to the lateral septum. *Brain Res.* **273**, 307–317 (1983).
50. E. M. Stricker, J. A. Hosutt, J. G. Verbalis, Neurohypophyseal secretion in hypovolemic rats: Inverse relation to sodium appetite. *Am. J. Physiol.* **252**, R889–R896 (1987).
51. T. E. Whitmore, J. L. Holloway, C. E. Lofton-Day, M. F. Maurer, L. Chen, T. J. Quinton, J. B. Vincent, S. W. Scherer, S. Lok, Human secretin (SCT): Gene structure, chromosome location, and distribution of mRNA. *Cytogenet. Genome Res.* **90**, 47–52 (2000).
52. P. Li, T. M. Chang, W. Y. Chey, Secretin inhibits gastric acid secretion via a vagal afferent pathway in rats. *Am. J. Physiol.* **275**, G22–G28 (1998).
53. J. D. Gardner, Receptors for gastrointestinal hormones. *Gastroenterology* **76**, 202–214 (1979).
54. J. Y. S. Chu, C. Y. Y. Cheng, V. H. Y. Lee, Y. S. Chan, B. K. C. Chow, Secretin and body fluid homeostasis. *Kidney Int.* **79**, 280–287 (2011).
55. L. T. O. Lee, J. Y. S. Chu, I. P. Y. Lam, F. K. Y. Siu, H. Vaudry, B. K. C. Chow, An indispensable role of secretin in mediating the osmoregulatory functions of angiotensin II. *FASEB J.* **24**, 5024–5032 (2010).
56. J. Bai, K. Duraisamy, S. O. K. Mak, A. Allam, J. Ajarem, Z. Li, B. K. C. Chow, Role of SCTR/AT1aR heteromer in mediating ANGII-induced aldosterone secretion. *PLOS ONE* **14**, e0222005 (2019).
57. J. Bai, B. K. C. Chow, Secretin is involved in sodium conservation through the renin-angiotensin-aldosterone system. *FASEB J.* **31**, 1689–1697 (2017).
58. V. H. Y. Lee, L. T. O. Lee, J. Y. S. Chu, I. P. Y. Lam, F. K. Y. Siu, H. Vaudry, B. K. C. Chow, An indispensable role of secretin in mediating the osmoregulatory functions of angiotensin II. *FASEB J.* **24**, 5024–5032 (2010).
59. S. Afroze, F. Meng, K. Jensen, K. M. Daniel, K. Rahal, P. Onori, E. Gaudio, G. Alpini, S. S. Glaser, The physiological roles of secretin and its receptor. *Ann. Transl. Med.* **1**, 29 (2013).
60. W. Y. Chey, T.-M., Secretin, 100 years later. *J. Gastroenterol.* **38**, 1025–1035 (2003).
61. D. Dogrukol-Ak, F. Tore, N. Tuncel, Passage of VIP/PACAP/secretin family across the blood-brain barrier: Therapeutic effects. *Curr. Pharm. Des.* **10**, 1325–1340 (2004).
62. K. Lossow, W. Meyerhof, M. Behrens, Sodium imbalance in mice results primarily in compensatory gene regulatory responses in kidney and colon, but not in taste tissue. *Nutrients* **12**, 995 (2020).
63. C. Duc, N. Farman, C. M. Canessa, J. P. Bonvalet, B. C. Rossier, Cell-specific expression of epithelial sodium channel alpha, beta, and gamma subunits in aldosterone-responsive epithelia from the rat: Localization by in situ hybridization and immunocytochemistry. *J. Cell Biol.* **127**, 1907–1921 (1994).
64. K. Kunzelmann, M. Mall, Electrolyte transport in the mammalian colon: Mechanisms and implications for disease. *Physiol. Rev.* **82**, 245–289 (2002).
65. S. S. Árnason, E. Skadhauge, Steady-state sodium absorption and chloride secretion of colon and coprodeum, and plasma levels of osmoregulatory hormones in hens in relation to sodium intake. *J. Comp. Physiol. B* **161**, 1–14 (1991).
66. N. D. Gallagher, D. D. Harrison, A. P. Skyring, Fluid and electrolyte disturbances in patients with long-established ileostomies. *Gut* **3**, 219–223 (1962).
67. G. L. Hill, J. C. Goligher, A. H. Smith, W. S. Mair, Long term changes in total body water, total exchangable sodium and total body potassium before and after ileostomy. *Br. J. Surg.* **62**, 524–527 (1975).
68. I. A. Gómez de Segura, Marijuan, P. Trillo, M. Picornell, R. Codoceo, J. Díaz, E. de Miguel, Changes in plasma levels of intestinal regulatory peptides following colonic resection in the rat. *Rev. Esp. Enferm. Dig.* **87**, 20–24 (1995).

Acknowledgments

Funding: This study was funded by the National Key Research and Development Program of China (2022ZD0207600 and 2020YFA0113600 to L.Z.), the National Natural Science Foundation of China (32070955 to L.Z. and 81971067 and U22A20301 to K.-F.S.), the Guangzhou Key Research Program on Brain Science (202007030012 to L.Z. and 202206060001 and 202007030011 to L.S.), the Guangdong Natural Science Foundation (2019A1515011772 to L.Z.), and the Hong Kong Government (GRF HKU17113120 and HKU17127718 to B.K.C.C.). **Author**

contributions: Y.Liu. and J.-a.W. designed all experiments and performed molecular, behavioral, histological, and in vivo imaging assays, as well as the data analysis. Z.L. performed the electrophysiological studies. J.C. and S.W. assisted in the behavioral assays. Y.Luo., S.O.K.M., and F.Z. helped the animal model and surgeries. Y.Y. helped the measurement of heart rate. The manuscript was written by Y.Liu., J.-a.W., and L.Z., with inputs from all authors. L.S., B.K.C.C., and L.Z. secured the funding, revised the manuscript, and supervised all experiments. All authors approved this manuscript. **Competing interests:** The authors declare that they have no competing interests. **Data and materials availability:** All data needed to evaluate the conclusions in the paper are present in the paper and/or the Supplementary Materials.

Submitted 16 June 2022
Accepted 17 January 2023
Published 15 February 2023
10.1126/sciadv.add5330